EARTH SCIENCES

10.1126/sciadv.1501671

Low-temperature plasticity of olivine revisited with in situ TEM nanomechanical testing

Hosni Idrissi,[1,2] Caroline Bollinger,[3] Francesca Boioli,[4]* Dominique Schryvers,[1] Patrick Cordier[4]†

The rheology of the lithospheric mantle is fundamental to understanding how mantle convection couples with plate tectonics. However, olivine rheology at lithospheric conditions is still poorly understood because experiments are difficult in this temperature range where rocks and mineral become very brittle. We combine techniques of quantitative in situ tensile testing in a transmission electron microscope and numerical modeling of dislocation dynamics to constrain the low-temperature rheology of olivine. We find that the intrinsic ductility of olivine at low temperature is significantly lower than previously reported values, which were obtained under strain-hardened conditions. Using this method, we can anchor rheological laws determined at higher temperature and can provide a better constraint on intermediate temperatures relevant for the lithosphere. More generally, we demonstrate the possibility of characterizing the mechanical properties of specimens, which can be available in the form of submillimeter-sized particles only.

The rheology of the lithospheric mantle is fundamental to understanding how mantle convection couples with plate tectonics (*1*). There is a growing consensus that the rheology of olivine at low temperatures relevant for the lithospheric mantle cannot be extrapolated from rheological laws established from experiments at high temperature (ca. >1300 K) (*2*, *3*). However, it has been shown recently that deforming olivine in the laboratory becomes extremely difficult when temperatures approach 1000 K (*2*, *4*). Not only does olivine becomes increasingly brittle but also a steady state becomes difficult to reach and instabilities often develop. Below 600 K, data are scarce (see Fig. 1) and constitutive equation adjustments rely mostly on the pioneering study of Evans and Goetze (*5*). These measurements are based on indentation, a technique that is simple to use but rather difficult to interpret because strain rate, pressure, and microstructures are poorly constrained and very heterogeneous. With recently developed high-pressure deformation apparatus like the D-DIA, the ductile field of olivine has been extended by applying larger confining pressures between 4 and 10 GPa (*6*, *7*). Long *et al.* (*7*) have shown that, in the low-temperature range, strain hardening dominates plasticity. Indeed, when olivine is loaded at high laboratory strain rates at low temperature where dislocation mobility is low, the only solution to produce enough strain is to increase the dislocation density. However, this results in a further decrease of the effective mobility due to back stress and dislocation interactions and then to a further need for increasing the dislocation density. Indentation and high-pressure data have recently been questioned by the results obtained at lower pressure (1 to 2.5 GPa) by Druiventak *et al.* (*8*), who found olivine to be significantly weaker than previously suggested. However, the discrepancy between published studies is large because, for instance, yield strengths measured at room temperature span a 4-GPa-wide interval. This suggests that laboratory data obtained at low temperature overestimate the intrinsic strength of olivine and are not suitable for extrapolation to natural conditions. There is thus a need to clarify the intrinsic strength of olivine at low temperature.

Another approach to rheology has been recently proposed, which is based on the incorporation of elementary deformation mechanisms into physics-based models (*9*). Multiscale numerical modeling emphasizes the critical role of the mobility of dislocations. The mobility of dislocations results from a complex interplay between stress and thermal activation. Despite the importance of dislocation mobility, direct measurements are rare and mostly limited to soft metals that can be deformed in situ in the transmission electron microscope (TEM). Here, we propose a novel approach to directly measuring dislocation mobility in olivine at room temperature, hence providing a very efficient lever arm effect to anchor rheological laws (see Fig. 1).

The most common technique to prevent brittle fracture and to enhance ductility is to apply a confining pressure, which prevents the opening and propagation of cracks. However, with the advent of nanotechnologies, it is possible to investigate the mechanical properties of very small samples, which exhibit specific properties including very high toughness (*10*–*17*). Indeed, the behavior of real solids is far from the theoretical properties that can be expected from perfect solids. For instance, the ideal tensile strength of olivine is of the order of $E/10$ (E being Young's modulus), that is, slightly below 20 GPa. However, the fracture toughness of real olivine is much lower because it is controlled by the presence of internal flaws. Griffith (*18*) has shown that the presence of a critical crack of length a reduces the fracture stress σ_f in such a way that $\sigma_f\sqrt{a}$ remains a constant. The use of very small samples places very strong geometrical constraints on the size of the defects the sample may contain. Here, we use beams with the smallest dimension (the thickness) being of the order of 200 nm. Careful sample preparation with ion beams and sample examination in the TEM guarantee that internal flaws are at the nanometer level, which raises the fracture stress to levels similar to that of the flow stress expected at room temperature in olivine.

Here, we present in situ TEM uniaxial tensile experiments performed on submicrometer beams of olivine using the single-tilt PI 95 TEM PicoIndenter from Hysitron Inc. (*19*) and a special push-to-pull (PTP) device (*20*, *21*) designed for in situ quantified TEM nanotensile tests (Fig. 2; see Materials and Methods and the Supplementary Materials

[1]Electron Microscopy for Materials Science (EMAT), University of Antwerp, Groenenborgerlaan 171, B-2020 Antwerp, Belgium. [2]Institute of Mechanics, Materials and Civil Engineering, Université catholique de Louvain, Place Sainte Barbe 2, B-1348 Louvain-la-Neuve, Belgium. [3]Bayerisches Geoinstitut, University of Bayreuth, D-95440 Bayreuth, Germany. [4]Unité Matériaux et Transformations, UMR 8207 CNRS/Université Lille 1, F-59655 Villeneuve d'Ascq, France.
*Present address: Institut Lumière Matière, UMR 5306 CNRS/Université Lyon 1, F-69622 Villeurbanne, France.
†Corresponding author. E-mail: patrick.cordier@univ-lille1.fr

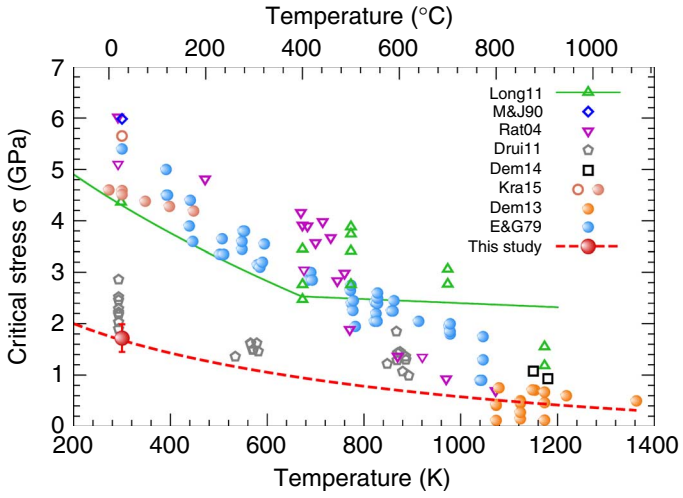

Fig. 1. Critical stress for plastic flow as a function of temperature. The red circle was obtained by including our in situ dislocation velocity measurements in our dislocation dynamics (DD) numerical model. The other points indicate experimental measurements taken from different sources in literature [E&G79 (*5*); M&J90 (*31*); Rat04 (*6*); Drui11 (*8*); Long11 (*7*); Dem13 (*2*); Dem14 (*32*); Kra15 (*36*)]. Full (empty) symbols are used to visualize mechanical data obtained by deforming single-crystal (polycrystalline) olivine samples. The new rheological law for olivine single crystals is shown with a dashed line.

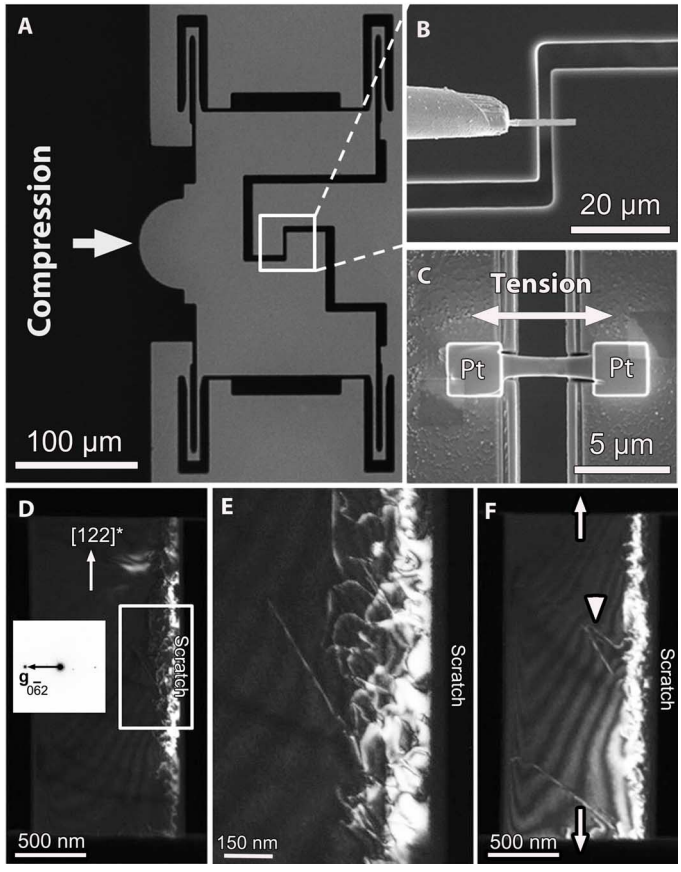

Fig. 2. In situ TEM nanomechanical testing. (**A**) Optical image of the PTP device used for in situ TEM tensile experiments. The compression of the semicircular end in (A) induces uniaxial tension in the middle gap shown in (B) and (C). (**B** and **C**) Scanning electron microscope (SEM) images showing the transfer of an FIB-prepared olivine sample onto the PTP device and the mounting of the sample in the middle gap using electron beam–deposited platinum (Pt), respectively. (**D**) WBDF-TEM image of the olivine sample DefOl-4 mounted on the PTP device before deformation. The scratch and the pulling direction are perpendicular to the (112) plane. The sample is oriented in a two-beam condition with the vector $\mathbf{g} = 0\bar{6}2$ perpendicular to the pulling direction. (**E**) Zoom on the damaged layer underneath the polished surface surrounded by the rectangle in (D). Several dislocation loops can be observed. (**F**) WBDF-TEM image showing the nucleation of a dislocation loop (white arrowhead) in the (110) plane from the damaged layer during in situ TEM straining. The pulling direction is indicated by white arrows in (F).

for more details). Samples with dimensions of about 4 × 1 × 0.2 µm were machined with a focused ion beam (FIB) from an oriented single crystal of San Carlos olivine. At low temperature, the plasticity of olivine is dominated by glide of [001] dislocations on {110} and (100) planes (*22*). We oriented our beams with the tensile direction perpendicular to the (122) plane. With this orientation, the resolved shear stress on the [001](110) slip system is close to maximum (Schmid factor, 0.47). The slip plane is at ca. 130° from the viewing direction, which allows good visibility on the gliding dislocations. Dislocations are imaged during the experiment in weak-beam dark-field (WBDF) conditions using the $0\bar{6}2$ diffraction vector. Tensile stress is applied using the load control mode. Load is increased to a given value, which is maintained constant for several minutes before unloading. During the plateau, dislocation motion is observed and characterized (hence, under a known and constant applied stress). Then, the sequence is repeated again at a different stress. Dislocations are nucleated from dislocation loops left below the surface by mechanical polishing (Fig. 2; see also the Supplementary Materials). The loops expand, pulled by the most rapid, nonscrew segments, which leave slower screw segments (Fig. 3, A to F) that propagate across the sample. In a material where dislocation velocity is very anisotropic, fast characters produce little plastic strain. Their role is to create the slow characters, which then propagate and produce the strain. That is why in this study, we focus on the measurement of the velocity of the screw segments, which control plasticity in bulk olivine. Figure 3G shows the results of the measurements describing the influence of stress on the mobility at 300 K of a screw dislocation of length 0.8 µm in olivine.

Although stress and displacements (hence, strain) are known during the entire experiments, care should be taken in how they are used. Indeed, in small-scale experiments, the mechanical properties may be strongly controlled by the nucleation of dislocations (*10*, *12*, *23*–*26*). Here, we do observe that emission of loops from surface damage is a controlling factor. Indeed, the stresses that are involved in our experiments correspond to the critical stresses of activation of Frank-Read sources of dimensions ranging from 30 to 60 nm (see the Supplementary Materials), in perfect agreement with what we observe. Our experiments give us access to a fundamental parameter: the velocity of screw dislocations (Fig. 3G).

To determine the stress-strain curves for olivine at room temperature, we introduce the velocity of dislocations measured here into a DD numerical model, which has been recently adapted to olivine (*27*). This method is based on the calculation of the forces acting on dislocations by using linear elasticity theory. It provides an accurate description of the long-range elastic strain field induced by dislocations (see Fig. 4A), their interactions, and the interaction of these line defects with an external stress field (*28*). At each step, dislocations are moved

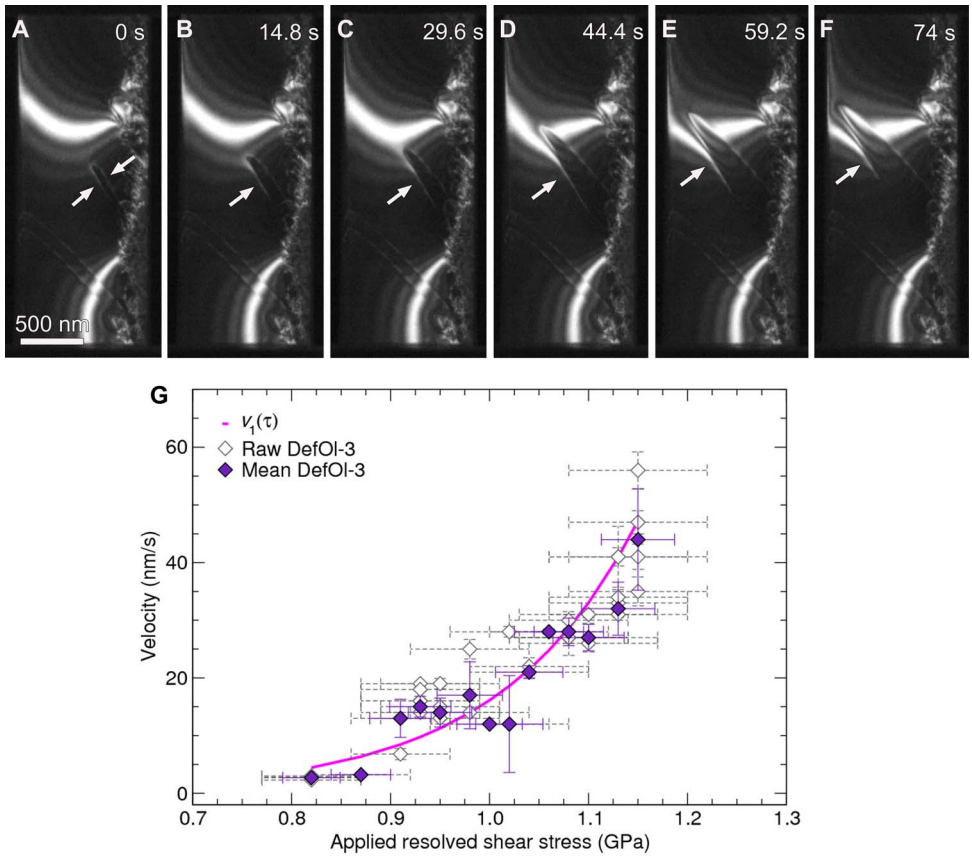

Fig. 3. TEM measurements of the mobility of screw dislocations. (**A** to **F**) Video frames captured during the in situ deformation of sample DefOI-3 under a constant load of 384 μN (resolved shear stress, 0.89 GPa). A movie is available in the Supplementary Materials. The loop expands from the scratch and develops, allowing propagation of the screw segment (arrowed) to be followed across the specimen. A table describing the different experiments is included in the Supplementary Materials. (**G**) Velocities (in nm s^{-1}) of screw dislocations versus stress (in GPa). Data from the DefOI-3 experiment are presented for all raw measurements (empty diamonds) and weighted means at each stress (indigo diamonds). $v_1(\tau)$ is the fit introduced in the DD model (see the Supplementary Materials). These velocities correspond to a screw dislocation segment of length 0.8 μm.

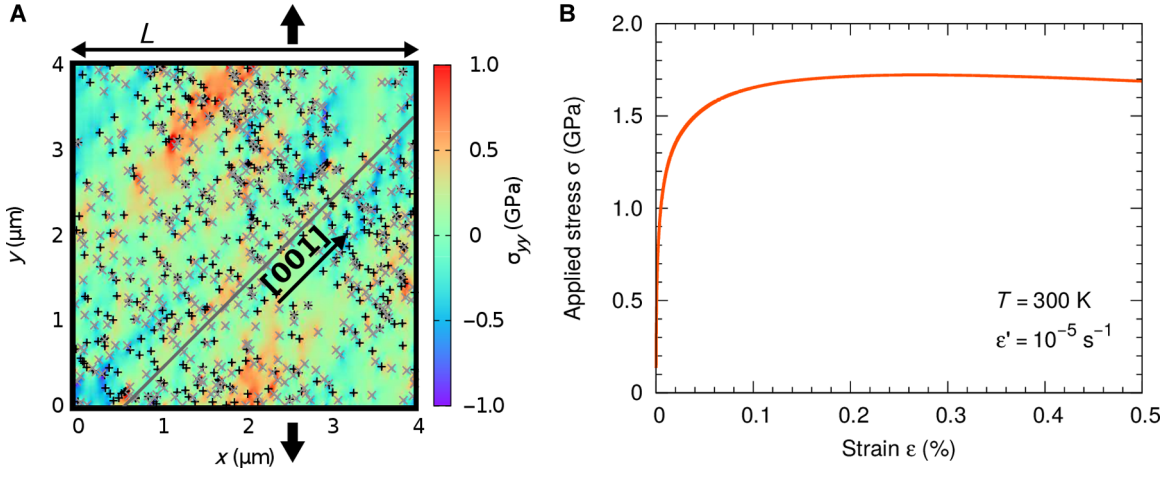

Fig. 4. Dislocation dynamics simulations. (**A**) Sketch of the DD simulation box. Single-slip conditions and uniaxial loading are applied along the *y* direction (loading direction). The angle between the loading axis and glide direction for the easiest [001](110) slip system is 45°. Dislocations (plus or x symbols) are superimposed on a color background, which represents the component σ_{yy} of the stress field induced by the dislocation microstructure and the imposed external forces. (**B**) Stress-strain curve obtained from the DD numerical model by using the dislocation velocity inferred from the PTP experiments.

in the direction of the forces according to their mobility laws (here from our measurements). In the 2.5-dimensional (2.5D) DD model (*29*), dislocations are modeled by parallel straight segments perpendicular to a 2D reference plane (see Fig. 4A). Additional rules are included to reproduce important 3D dislocation mechanisms (the 2.5D model is thus a 2D model able to describe a 3D behavior), such as dislocation multiplication or junction formation [more details in Boioli *et al.*'s study (*27*)].

Here, we model a simple tensile test on a single crystal of olivine with the easiest [001](110) slip system oriented at 45° from the loading axis. Hence, we obtain the lowest bound for the rheology of olivine under those conditions because polycrystalline plasticity would also take into account the contribution of harder slip systems as well as grain boundary contribution (olivine does not have enough slip systems to fulfil the von Mises criterion). However, Fig. 1 shows that the polycrystalline data (Dem14) do not differ much from the easy slip–oriented single-crystal data (Dem13). Results from Evans and Goetze (*5*) lead to the same conclusion. The mobility law used in the model is the one determined experimentally and described in Fig. 3G. Figure 4B shows the stress-strain curve from the DD simulation. The flow stress in the steady-state regime is 1.72 ± 0.27 GPa. This value is significantly lower than the values inferred from experiments on polycrystals at high pressure and from those of Evans and Goetze (*5*), which were also obtained on single crystals. The present work suggests that rheological laws based on previous low-temperature data need to be significantly reconsidered because they strongly overestimate the intrinsic olivine strength at low temperature. We propose a new rheological law for single-crystal olivine deformed in easy slip, which is consistent with both single-crystal experiments (*2*) at ca. 0.5 T_m (T_m is the melting temperature, that is, for olivine, Fo90 ≈ 1973 K) and our results at room temperature (that is, 0.15 T_m). Mechanical properties of materials that exhibit a large resistance to deformation are generally well described by introducing the dependence of strain rates $\dot{\varepsilon}$ on stress σ within the exponential term

$$\dot{\varepsilon} = A \exp\left(-\frac{Q}{RT}\left(1-\left(\frac{\sigma}{\sigma_0}\right)^p\right)^q\right) \quad (1)$$

where R is the gas constant, Q is the activation energy, and A, σ_0, p, and q are empirical parameters. Here, we set $p = 0.5$ and $q = 2$, similarly to Demouchy *et al.* (*2*), and we fit the parameters A, Q, and σ_0 in Eq. 1 to reproduce the new evidence of olivine strength at low temperature, as illustrated by the dashed line in Fig. 1. The values of the fitted parameters are reported in Table 1.

To summarize, conventional experiments where confining pressure is applied to enhance plasticity at low temperature are not adapted to describe the rheology of olivine at low strain rate. In laboratory tests, olivine is strongly driven. It strongly strain-hardens, and its strength, controlled by dislocations interactions, is overestimated. We emphasize here an important issue for the extrapolation of laboratory data to nature: not only must the same mechanisms operate, but it is also important to make sure that comparable microstructures are involved. We apply nanomechanical testing to investigate directly the micromechanics of plasticity in olivine at room pressure and temperature. We propose a new rheological law, which can describe a lower bound for the rheology of olivine in the lithosphere. We provide an experimental basis for recent models (*30*), which suggest that anhydrous olivine is ductile enough to account for the rheology of the lithosphere.

Table 1. Values of the parameters defining the new rheological law reported in Eq. 1 and shown in Fig. 1 (dashed red line).

A	*Q*	σ_0	*p*	*q*
1×10^6 (s^{-1})	566±74 (kJ/mol)	3.8±0.7 (GPa)	0.5	2

MATERIALS AND METHODS

Nanomechanical testing

The experiments were performed in load-controlled compression mode using a conductive diamond flat punch indenter in the PI 95 TEM PicoIndenter from Hysitron Inc. A special microelectromechanical system device called PTP was used. Because of four identical springs distributed symmetrically at the corners of this device, the compression (push) of the semicircular end of the PTP device using the flat punch indenter is converted into a uniaxial tensile loading (pull) on the middle gap of the PTP device (Fig. 2). The springs are arranged such that the force acting on them is parallel to the force on the tensile specimen. Here, the stiffness of the springs was equal to 150 N/m. Freestanding olivine beams were cut by FIB in an oriented single crystal of San Carlos olivine and transferred to the PTP device using an Omniprobe micromanipulator on an FEI dual beam FIB/SEM instrument. The beams were then attached to the PTP device using electron beam–deposited Pt as shown in Fig. 2. The velocities of the screw dislocations nucleated from the scratch have been measured as a function of increasing stress applied on the samples in the load control mode (see the Supplementary Materials).

Transmission electron microscopy

The in situ tensile tests were run in an FEI Osiris microscope operating at 200 kV and equipped with a high-brightness XFEG (field-emission gun) source. The instrument is fully remote-controlled from an operator room outside the room of the microscope, leading to a higher stability during the in situ TEM nanomechanical testing experiments. Video sequences were recorded by a Gatan UltraScan CCD camera with a postspecimen shutter. Here, the measurement of the velocity of the dislocations required accurate determination of the position of the dislocations in the frames extracted from the recoded videos. These videos have been thus recorded with a high spatial resolution of 2048 × 2048 at a frame rate of 5 fps to observe the slow movement of the dislocations at constant load. Electron dose rate of 12 $e^-/Å^2 \cdot s$ with a beam current of 3.87 nA was used to record in situ the movement of the dislocations. The effect of the electron beam on the mobility of the dislocations was not observed (see the Supplementary Materials).

DD modeling

DD simulations were performed in single slip, [001](110), and uniaxial loading conditions. A constant strain rate of 1×10^{-5} s^{-1} was applied for the tensile test. The simulation area is a square of size $L = 4$ μm, and the initial dislocation density is 12×10^{12} m^{-2}. The dislocations are perpendicular to the reference plane and ideally infinite. Their Burgers vector lies in the reference plane and defines the slip direction, as sketched in Fig. 4A. Here, we took the slip direction inclined by 45° with respect to the loading axis, the y direction, to obtain the maximum resolved shear stress on the slip plane (Schmid's factor, 0.5). Dislocations

are moved along the slip plane direction according to the mobility law extracted from the here-presented experiments. In particular, we fitted the experimental data with an exponential fit. The resulting velocity is given by $v_i = A_i \exp(c_i\tau^*)$, where τ^* is the effective stress given by the sum of the applied and the internal stresses, whereas c_i and A_i are constants fitted on the experimental data. Data shown in Fig. 3 for DefOl-3 lead to $c_i = 7.17 \pm 0.55$ GPa^{-1} and $A_i = e^{-4.39 \pm 0.56}$ nm s^{-1} (more information in the Supplementary Materials). We notice that the description of the velocity at low stresses does not influence significantly the DD because the plastic flow is controlled by the fastest dislocations, that is, by the dislocations that sustain high stress values, which are well characterized by the experiments.

SUPPLEMENTARY MATERIALS

Supplementary material for this article is available at http://advances.sciencemag.org/cgi/content/full/2/3/e1501671/DC1

Materials and Methods

Fig. S1. Stereographic plot (planes) of the beam strained in the microscope as viewed along the electron beam direction.

Fig. S2. FIB preparation of olivine specimens for in situ TEM nanomechanical testing.

Fig. S3. SEM measurements of the cross-sectional area of the tensile sample.

Fig. S4. True stress–true strain curve of olivine sample deformed elastically up to 3.4 GPa and 0.021 strain.

Fig. S5. WBDF-TEM imaging of dislocations.

Fig. S6. Force cycles applied to the sample "DefOl-3."

Fig. S7. Experimental procedure used to measure the velocity of dislocations at low resolved shear stresses in sample "DefOl-4."

Fig. S8. Critical stress for source opening as a function of the loop radius.

Fig. S9. Snapshots from in situ TEM tensile experiment at constant load of 365 μN applied on sample "DefOl-2."

Fig. S10. Calculation of the image forces on a dislocation parallel to the free surfaces of a 200-nm-thick foil (green band).

Fig. S11. Example of the measurement of the velocity of a screw dislocation (segment arrowed) within a single cycle.

Fig. S12. Dislocation velocity as a function of the resolved shear stress: influence of the fit on the DD results.

Fig. S13. Influence of the initial dislocation density on the DD results.

Fig. S14. Influence on the dislocation length on the DD results.

Fig. S15. Histograms of the stresses experienced by the dislocations in the DD simulations and of the resulting strains.

Table S1. Intensity (and dhkl) of the most efficient reflections in olivine (calculated with the "electron diffraction" software).

Table S2. Summary of the in situ TEM tensile experiments achieved in the present study.

Movie S1. The in situ deformation of sample DefOl-3 under a constant load of 360 μN (resolved shear stress, 0.82 GPa).

References (*33*–*35*)

REFERENCES AND NOTES

1. D. L. Kohlstedt, B. Evans, S. J. Mackwell, Strength of the lithosphere: Constraints imposed by laboratory experiments. *J. Geophys. Res.* **100**, 17587–17602 (1995).
2. S. Demouchy, A. Tommasi, T. Boffa Ballaran, P. Cordier, Low strength of Earth's uppermost mantle inferred from tri-axial deformation experiments on dry olivine crystals. *Phys. Earth Planet. In.* **220**, 37–49 (2013).
3. S. Zhong, A. Watts, Lithospheric deformation induced by loading of the Hawaiian Islands and its implications for mantle rheology. *J. Geophys. Res.* **118**, 6025–6048 (2013).
4. S. Demouchy, S. E. Schneider, S. J. Mackwell, M. E. Zimmerman, D. L. Kohlstedt, Experimental deformation of olivine single crystals at lithospheric temperatures. *Geophys. Res. Lett.* **36**, L04304 (2009).
5. B. Evans, C. Goetze, The temperature variation of hardness of olivine and its implication for polycrystalline yield stress. *J. Geophys. Res.* **84**, 5505–5524 (1979).
6. P. Raterron, Y. Wu, D. J. Weidner, J. Chen, Low-temperature olivine rheology at high pressure. *Phys. Earth Planet. In.* **145**, 149–159 (2004).
7. H. Long, D. J. Weidner, L. Li, J. Chen, L. Wang, Deformation of olivine at subduction zone conditions determined from in situ measurements with synchrotron radiation. *Earth Planet. Sci. Lett.* **186**, 23–35 (2011).
8. A. Druiventak, C. A. Trepmann, J. Renner, K. Hanke, Low-temperature plasticity of olivine during high stress deformation of peridotite at lithospheric conditions—An experimental study. *Earth Planet. Sci. Lett.* **311**, 199–211 (2011).
9. P. Cordier, J. Amodeo, P. Carrez, Modelling the rheology of MgO under Earth's mantle pressure, temperature and strain rates. *Nature* **481**, 177–181 (2012).
10. M. D. Uchic, D. M. Dimiduk, J. N. Florando, W. D. Nix, Sample dimensions influence strength and crystal plasticity. *Science* **305**, 986–989 (2004).
11. D. S. Gianola, C. Eberl, Micro- and nanoscale tensile testing of materials. *JOM* **61**, 24–35 (2009).
12. S. H. Oh, M. Legros, D. Kiener, G. Dehm, In situ observation of dislocation nucleation and escape in a submicron Al single-crystal. *Nat. Mater.* **8**, 95–100 (2009).
13. J. R. Greer, J. T. M. De Hosson Plasticity in small-sized metallic systems: Intrinsic versus extrinsic size effect. *Progr. Mater. Sci.* **56**, 654–724 (2011).
14. H. Idrissi, B. Wang, M. S. Colla, J. P. Raskin, D. Schryvers, T. Pardoen, Ultra high strain hardening in thin palladium films with nanoscale twins. *Adv. Mater.* **23**, 2119–2122 (2011).
15. D. Kiener, A. M. Minor, Source truncation and exhaustion: Insights from quantitative in situ TEM tensile testing. *Nano Lett.* **11**, 3816–3820 (2011).
16. Q. Yu, L. Qi, K. Chen, R. K. Mishra, J. Li, A. M. Minor, The nanostructured origin of deformation twinning. *Nano Lett.* **12**, 887–892 (2012).
17. M. Legros, In situ mechanical TEM: Seeing and measuring under stress with electrons. *C. R. Phys.* **15**, 224–240 (2014).
18. A. A. Griffith, The phenomena of rupture and flow in solids. *Philos. Trans. R. Soc. Lond. A* **221**, 163–198 (1921).
19. A. M. Minor, S. A. Syed Asif, Z. Shan, E. A. Stach, E. Cyrankowski, T. J. Wyrobek, O. L. Warren, A new view of the onset of plasticity during the nanoindentation of aluminium. *Nat. Mater.* **5**, 697–702 (2006).
20. C. Chisholm, H. Bei, M. B. Lowry, J. Oh, S. A. Syed Asif, O. L. Warren, Z. W. Shan, E. P. George, A. M. Minor, Dislocation starvation and exhaustion hardening in Mo alloy nanofibers. *Acta Mater.* **60**, 2258–2264 (2012).
21. H. Idrissi, A. Kobler, B. Amin-Ahmadi, M. Coulombier, M. Galceran, J.-P. Raskin, S. Godet, C. Kübel, T. Pardoen, D. Schryvers, Plasticity mechanisms in ultrafine grained freestanding aluminum thin films revealed by in situ transmission electron microscopy nanomechanical testing. *Appl. Phys. Lett.* **104**, 101903(1)–101903(5) (2014).
22. C. B. Raleigh, Mechanisms of plastic deformation of olivine. *J. Geophys. Res.* **73**, 5391–5406 (1968).
23. S. H. Oh, M. Legros, D. Kiener, P. Gruber, G. Dehm, In situ TEM straining of single crystal Au films on polyimide: Change of deformation mechanisms at the nanoscale. *Acta Mater.* **55**, 5558–5571 (2007).
24. Z. W. Shan, R. K. Mishra, S. A. Syed Asif, O. L. Warren, A. M. Minor, Mechanical annealing and source-limited deformation in submicrometre-diameter Ni crystals. *Nat. Mater.* **7**, 115–119 (2008).
25. M. D. Uchic, P. A. Shade, D. M. Dimiduk, Micro-compression testing of fcc metals: A selected overview of experiments and simulations. *JOM* **61**, 36–41 (2009).
26. L. Y. Chen, M.-R. He, J. Shin, G. Richter, D. S. Gianola, Measuring surface dislocation nucleation in defect-scarce nanostructures. *Nat. Mater.* **14**, 707–713 (2015).
27. F. Boioli, P. Carrez, P. Cordier, B. Devincre, M. Marquille, Modelling the creep properties of olivine by 2.5-D dislocation dynamics simulations. *Phys. Rev. B* **92**, 014115 (2015).
28. J. P. Hirth, J. Lothe, *Theory of Dislocations* (Wiley, New York, 1992).
29. D. Gómez-García, B. Devincre, L. Kubin, Dislocation patterns and similitude principle: 2.5D mesoscale simulations. *Phys. Rev. Lett.* **96**, 125503 (2006).
30. F. Boioli, P. Carrez, P. Cordier, B. Devincre, M. Marquille, Low steady state stresses in the cold lithospheric mantle inferred from dislocation dynamics models of dislocation creep in olivine. *Earth Planet. Sci. Lett.* **432**, 232–242 (2015).
31. C. Meade, R. Jeanloz, The strength of mantle silicates at high pressures and room temperature: Implications for the viscosity of the mantle. *Nature* **348**, 533–535 (1990).
32. S. Demouchy, A. Mussi, F. Barou, A. Tommasi, P. Cordier, Viscoplasticity of polycrystalline olivine experimentally deformed at high pressure and 900°C. *Tectonophysics* **623**, 123–135 (2014).
33. R. J. Angel, L. W. Finger, *SINGLE*: A program to control single crystal diffractometers. *J. Appl. Crystallogr.* **44**, 247–251 (2011).
34. U. F. Kocks, S. Argon, F. Ashby, *Thermodynamics and Kinetics of Slip* (Pergamon Press, Oxford, 1975).
35. S. L. Webb, The elasticity of the upper mantle orthosilicates olivine and garnet to 3 GPa. *Phys. Chem. Min.* **16**, 684–692 (1989).
36. K. Kranjc, Z. Rouse, K. M. Flores, P. Skemer, Low-temperature plastic rheology of olivine determined by nanoindentation. *Geophys. Res. Lett.* **43**, 176–184 (2015).

Acknowledgments: We thank T. Boffa Ballaran (Bayerisches Geoinstitut) for her help in orienting the crystals. **Funding:** H.I. acknowledges the IAP program of the Belgian State Federal Office for Scientific, Technical and Cultural Affairs, under contract no. P7/21, and Fund for Scientific Research (FWO) grant G012012N. P.C. and F.B. are supported by funding from the European Research Council under the Seventh Framework Programme (FP7), ERC grant N°290424—RheoMan. **Author contributions:** P.C. and C.B. designed the experiments with H.I. and D.S. C.B. oriented and prepared the samples. H.I. performed the in situ TEM nanomechanical testing experiments. C.B., H.I., and P.C. analyzed the data. F.B. performed the numerical simulations. All authors discussed and interpreted the results. P.C. wrote the paper with feedback and contributions of all co-authors. **Competing interests:** The authors declare that they have no competing interests. **Data and materials availability:** All data needed to evaluate the conclusions in the paper are present in the paper and/or Supplementary Materials. Additional data related to this paper may be requested from the authors.

Submitted 20 November 2015
Accepted 27 January 2016
Published 11 March 2016
10.1126/sciadv.1501671

Citation: H. Idrissi, C. Bollinger, F. Boioli, D. Schryvers, P. Cordier, Low-temperature plasticity of olivine revisited with in situ TEM nanomechanical testing. *Sci. Adv.* **2**, e1501671 (2016).

ScienceAdvances
AAAS

Low-temperature plasticity of olivine revisited with in situ TEM nanomechanical testing

Hosni Idrissi, Caroline Bollinger, Francesca Boioli, Dominique Schryvers and Patrick Cordier (March 11, 2016)

Sci Adv 2016, 2:.
doi: 10.1126/sciadv.1501671